Applied Surface Science 539 (2021) 148236

Contents lists available at ScienceDirect

Applied Surface Science

journal homepage: www.elsevier.com/locate/apsusc

Adsorption of Evans blue and Congo red on carbon nanotubes and its influence on the fracture parameters of defective and functionalized carbon nanotubes studied using computational methods

Anna Jagusiak [a,*], Jakub Goclon [b], Tomasz Panczyk [c,*]

[a] Jagiellonian University Medical College, Faculty of Medicine, Chair of Medical Biochemistry, Kopernika 7, 31-034 Krakow, Poland
[b] University of Bialystok, Institute of Chemistry, ul. Ciolkowskiego 1K, 15-245 Bialystok, Poland
[c] Jerzy Haber Institute of Catalysis and Surface Chemistry, Polish Academy of Sciences, ul. Niezapominajek 8, 30-239 Krakow, Poland

ARTICLE INFO

Keywords:
Carbon nanotube
Congo red
Evans blue
Fracture
Shortening

ABSTRACT

This work addresses the problem of the modification of mechanical parameters of carbon nanotubes as a result of Congo red and Evans blue adsorption, functionalization of the nanotubes surfaces by carboxyl groups and generation of surface defects. The studies were also focused on the quantum chemical analysis of the effects of Evans blue adsorption on the properties of the nanotubes. We found that Evans blue is rather physisorbed than chemisorbed and it does not significantly affect the electronic state of the nanotubes. The molecular dynamics studies led to the conclusion that the nanotube chirality affects the fracture parameters substantially but the presence of the adsorbed Congo red/Evans blue mixture has only minor effect for the zigzag nanotubes. The effect is slightly bigger for the defective armchair nanotubes and significant fluctuations of the failure strain was observed. However, non defective armchair ones are also not sensitive to the adsorption of dyes. The presence of surface functionalization was generally found as negligible. The only exception were defective armchair nanotubes for which small changes (±5%) were found for the carboxylated nanotubes.

1. Introduction

In many application areas carbon nanotubes (CNT) need processing in order to make them soluble or dispersed in solvents or cut into shorter fragments [1,2]. For that purpose several methods were proposed and they are generally divided into gas phase or liquid phase processing [3]. The gas phase processing uses gas phase oxidants like oxygen, steam, ozone or carbon dioxide [4,5]. While the liquid phase processing requires treatment by strong alkali or acids [3,6] or even by a mixture of hydrogen peroxide and sulfuric acid [7]. All these chemical treatments lead either to functionalization of the nanotubes or to their shortening.

The mentioned approaches to chemical cutting of the nanotubes are currently well recognized and allow for precise tailoring of the nanotube length or nature, localization or the density of the functional groups. However, all of them require drastic chemical reaction conditions often associated with the emission of harmful byproducts. These problems can, of course, be minimized in various ways and one of them could be application of softer chemical reagents. The latter approach is possible, as shown in the recent papers by Jagusiak et al. [8,9] and it only involves adsorption of some bisazo dyes on carbon nanotubes and subsequent sonication of that reaction mixture. The studied dyes i.e. Congo red (CR) and Evans blue (EB) are well known as reagents in medical diagnostics - CR is used *in vivo* for the diagnosis of amyloidosis [10] while EB serves to determine the blood volume [11]. Thus, shortening of the nanotubes using these reagents could be particularly useful in the area of drug delivery, for instance [12].

The mechanism of chemical cutting of carbon nanotubes by adsorption of these bisazo dyes is however unknown. Experimental data show that bundles of as produced nanotubes after adsorption of a mixture of CR and EB and sonication are shortened to an average lengths of 100–300 nm. The same sort of nanotubes with sodium cholate as a dispersant did not reveal shortening after sonication. Moreover, microscopy analysis shows that nanotubes break at places where CR/EB clusters were adsorbed [8]. This suggests strong chemical interaction of dyes with the nanotubes leading to strong weakening of their mechanical properties. On the other hand, CR and EB tend to form mixed supramolecular ribbon-like clusters [8,13] and microscopy studies show that those large clusters are attached to nanotube surface at some places

* Corresponding authors.
E-mail addresses: anna.jagusiak@uj.edu.pl (A. Jagusiak), tomasz.panczyk@ikifp.edu.pl (T. Panczyk).

https://doi.org/10.1016/j.apsusc.2020.148236
Received 23 September 2020; Received in revised form 19 October 2020; Accepted 20 October 2020
Available online 26 October 2020

and are separated from each other. So, it is also possible that nanotubes are cut mechanically without involving changes of the electronic structure and large masses of CR/EB clusters simply help in absorption of the mechanical energy coming from sonication.

Thus, the aim of this study is an attempt to explain the observed phenomena using computational methods. First, we analyzed interaction of EB with (17,0) carbon nanotube using the first principles DFT calculations. The choice of such a system is dictated by the experimental observations. Thus, it was observed that CR alone leads to dispersion of bundles of carbon nanotubes, however, EB molecule is necessary to observe their shortening [8,9]. The chirality of the nanotube, in turn, was adjusted according to the determined diameter of the nanotubes studied experimentally. This system was subjected to geometry optimization, determination of the density of states and electron charge transfer. Because the size of such a system was large and computation time long these quantum chemical studies were carried out for the EB/CNT(17,0) system only.

The mechanical parameters of nanotubes were based on the determination of fracture parameters of the nanotubes using classical molecular dynamics simulations, MD. The key component of such a methodology is a proper choice of an adequate force field. Thus, for the carbon nanotube we took a well known and thoroughly verified AIREBO force field [14] and for the dyes molecules we used the generalized amber force field, gaff [15]. This combination of force fields was additionally verified by the comparison of the EB geometry on the CNT surface with the geometry obtained from the quantum chemical DFT studies.

The quantum chemical computations concerning the effects of other combinations of systems parameters like presence of explicit solvent, Congo red molecule, surface defects etc were not carried out. This is because such systems are not tractable by DFT methods due their large size. Instead, we utilized the classical MD simulations assuming that the agreement between these methods, observed in the case of EB/CNT (17,0) geometry, will be preserved for the other systems. The classical MD studies were thus focused on the effects of such factors like presence of surface functional groups and surface defects on the fracture parameters with and without the adsorbed CR/EB on the CNT surface. As the functional group we studied the carboxyl group which is very common also in the case of commercially available samples of CNTs. Also the CNT chirality was checked as this factor affects the fracture parameters of carbon nanotubes strongly.

2. Methods

2.1. Quantum chemical analysis of Evans blue adsorption on (17,0) carbon nanotube

First-principle DFT calculations were carried out using Quantum Espresso [16] code by applying ultrasoft-type pseudopotentials [17]. We have adopted the generalized gradient approximation (GGA) within the Perdew-Burke-Ernzerhof [18](PBE) exchange-correlation functional with Grimme's D3 dispersion corrections and a Becke-Johnson dumping function [19]. The Kohn-Sham orbitals were expanded using plane-waves with an energy cut-off of 30 Ry. Geometry optimizations were performed without any symmetry constraints using the Broyden-Fletcher-Goldfarb-Shanno (BFGS) quasi-newton algorithm [20], until all residual forces were smaller than 5 meV/Å. The total energy was minimized using the Hellman-Feynman forces. The supercell approximation was applied with the Brillouin zone sampling at the Γ point. The convergence criterion for the electronic self-consistent iteration was set to be lower than 1.4 meV. A Gaussian smearing scheme with a value of 0.01 Ry was applied to aid convergence. For density of states (DOS) calculations, a 1x1x6 Monkhorst-Pack [21] k-point mesh was applied. In addition, the peak width for broadening was set to 0.1 eV for better visualization of the DOS.

The single walled carbon nanotube with chirality (17,0) was fully relaxed with an optimized length of 38.439 Å (612 atoms), what corresponds to nine unit cells along the tube axis. The lateral size of the supercell has been set up to be larger than 11 Å to minimize the interaction between analyzed molecular system and its periodic images. To characterize the stability of EB on the CNT(17,0), the adsorption energy (E_{ads}) was calculated according to:

$$E_{ads} = E_{EB/CNT(17,0)} - (E_{EB} + E_{CNT(17,0)}) \quad (1)$$

where $E_{EB/CNT(17,0)}$ is the total energy of the mixed system and E_{EB} and $E_{CNT(17,0)}$ denote the total energy of the isolated EB molecule and the nanotube, respectively. A negative value of E_{ads} means that the adsorption process is energetically favorable.

The azo/hydrazone tautomerism of hydroxyazo compounds is very common phenomenon especially when an azo and hydroxy groups are in the orto position [22] as is in the case of EB molecule. The energies of the three possible tautomers of the isolated EB molecule were calculated using an orthorhombic supercell, where the k-space was sampled at the Γ only. All the figures were produced using the visualization programs VESTA [23] and XcrySDen. [24]

2.2. Molecular dynamics simulations

2.2.1. Definitions of the analyzed systems

In molecular dynamics simulations we studied two types of carbon nanotubes: zigzag (17,0) and armchair (10,10) which have almost the same diameter and length. The nanotubes were either functionalized by carboxyl groups distributed randomly on their sidewalls of left without any surface modification. The number of carboxyl groups was 2% of carbon atoms. We also checked the effect of hole defects on the nanotubes surfaces and the combination of carboxyl functionalization and the presence of hole defects simultaneously. Finally, the nanotubes were either covered by 50:50 mixture of Congo red and Evans blue or left without adsorption of dyes in order the compare these cases. Essential information concerning the analyzed systems are collected in Table 1.

2.2.2. Covalent sidewall functionalization of carbon nanotubes

Carboxyl groups were grafted into bare CNT according to the following procedure. First we determined point charges of non-dissociated COOH group using as a template the molecule shown in Fig. 1A. The RESP charges were determined using RESP/ESP charge derive server: https://upjv.q4md-forcefieldtools.org/REDServer-Development. The resulting point charges on each atom are available in the supporting information file 'template.mol2'. In the next step the template.mol2 file was processed by the ACPYPE python script [25], which uses various programs from the AmberTools [26] package, and the gaff [15] force field topology of the molecule was finally obtained. The resulting force field files, in human readable gromacs format [27], are available as the supporting information (files template_GMX.gro and template_GMX.itp).

The carboxyl groups were randomly distributed on the CNT sidewall in the amount of 2% of total number of carbon atoms. The functionalization was carried out by placing the COOH atoms from the template molecule (Fig. 1A) above a selected C atom in the CNT at the distance ca. 1.4 Å and taking all force field components of the template molecule which contained atoms from the COOH group. But the other carbon atoms from the template molecule were replaced by the atoms from the CNT. The hydrogen atoms did not belong to any bond, angle or dihedral so they were simply ignored, however the partial charges belonging to atoms other than COOH part in the template molecule were summed and the effective reversed charge was imposed on the carbon atom directly linked with the C atom from the COOH group.

Finally, both carbon atoms: that one being functionalized and the one belonging to the CNT group were prescribed to the group of CNT atoms controlled by the AIREBO potential [28,14]. The oxygens and hydrogen atoms from the COOH were described by the general amber

Table 1
Essential information concerning the systems studied using molecular dynamics simulations. A given system name consists of a core name: letter 'z' or 'a' meaning zigzag or armchair nanotube, and a number '0′ or '20′ meaning the number of CR and EB molecules adsorbed on the CNT surface. Additionally, the core name may be prefixed by a letter 'd' meaning that a given CNT in defected or suffixed by the letter 'c' meaning that the CNT surface is functionalized by carboxyl groups. The name may be prefixed by letter 'd' and at the same time suffixed by the letter 'c' meaning that a given system contains surface defected and at the same time is functionalized by carboxyl groups.

System core name	CNT chirality	CNT diameter, Å	CNT length, Å	number of CR molecules	number of EB molecules	number of water molecules
z0	(17,0)	13.3	58.2	0	0	1691
z20	(17,0)	13.3	58.2	20	20	3808
a0	(10,10)	13.6	57.8	0	0	1682
a20	(10,10)	13.6	57.8	20	20	3791

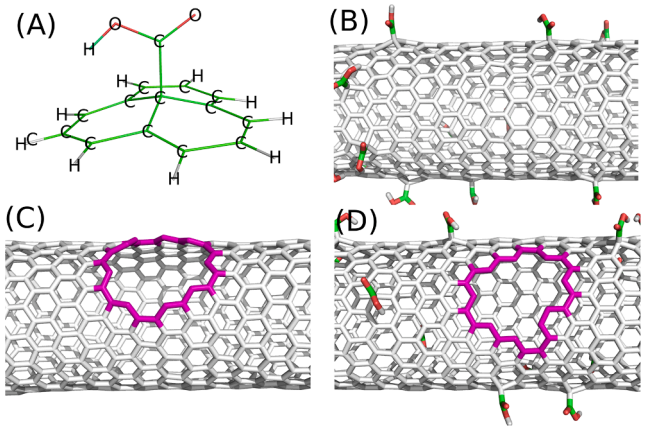

Fig. 1. (A) The template molecule used for the determination of point charges and the force field topology for covalent functionalization of the CNT by carboxyl groups. (B) Visualization of the CNT after covalent functionalization by carboxyl groups. (C) Visualization of the CNT after generation of the surface defect in a form of a hole. (D) Visualization of the CNT with covalent functionalization by carboxyl groups and with the surface defect generated.

force field, gaff. Thus, the C-C bond between CNT and COOH was able to dissociate but the COOH group itself was non cleavable. The systems with carboxylated nanotubes are denoted by the suffix 'c'.

2.2.3. Generation of defective nanotubes

The defects were generated by removing 11 neighboring carbon atoms so a hole in the nanotube wall was produced. Its size was approximately 6 × 11 Å so the dyes molecules could partially penetrate the hole but could not enter to the nanotube interior. The defect was localized in the middle of the CNT. The dangling bonds produced due to removal of carbon atoms were not saturated by hydrogens and the nanotube structure became altered due to rehybridization of carbon atoms at the edge of the hole. The rehybridization from sp2 to sp3 was done automatically by the bond order part of the AIREBO potential. Thus, effectively the dangling bonds were switched into sp3 carbon –CH terminal groups. The obtained in that way systems were denoted by the prefix 'd'. Fig. 1C, D shows the visualization of the considered nanotubes with the defects formed and also with the carboxyl functionalization.

2.2.4. Force fields

The carbon nanotubes and carbon atoms within the COOH groups were controlled by the reactive empirical bond order potential AIREBO. The other force field parameters from the COOH functional groups, Congo Red and Evans Blue molecules were described by the gaff [15] force field and the force field parameters for dyes molecules were obtained in the same manner like for the template molecule in Fig. 1A. The obtained force field files (in gromacs format) for both dyes are available as the supporting information files: Congo_red_GMX.gro, Congo_red_GMX.itp, Evans_blue_GMX.gro and Evans_blue_GMX.itp.

The AIREBO potential is responsible only for the internal structure of CNT thus the interaction of the CNT with dyes or water was described using non-bonded Lennard-Jones (LJ) and Coulomb (with particle particle mesh Ewald summation) potentials. The LJ parameters for carbon belonging to CNT were taken from the gaff force field. The water model was TIP3P and water molecules were treated as rigid bodies using the SHAKE algorithm.

2.2.5. Computations details

The molecular dynamics simulations were carried out using lammps MD program [29]. The force field parameters for CR, EB and the COOH groups generated by the ACPYPE script were formatted using a self designed program. The program computed the atomic positions of carbon atoms belonging to CNT, added the COOH groups to the CNT structure and placed dyes molecules, NaCl ions and water molecules in a way preventing from overlaps. The size of the simulation box was adjusted in such a way that CNT axis could be reproduced in z-direction in periodic images of the simulation box. Thus, effectively the CNT was assumed to be an infinitely long. The xy initial size of the simulation box was adjusted to the composition of the bulk. For pure saline solution the size was 17 × 17 Å. When the bulk contained dyes molecules the size was increased to 30 × 30 Å. The equilibration was carried out for 40 ns and during the equilibration we applied heating of the systems to 500 K and cooling to 298 K. The production runs were carried out at the temperature 298 K. The integration timestep was 2 fs during the equilibration cycles and it was reduced to 1 fs during application of the tensile load on the CNT.

Tensile properties of carbon nanotubes were determined by application of the axial load on the system and computation of the mechanical stress. These were done by application of the fix_deform and compute stress/atom routines implemented in lammps. The fracture analysis started after full equilibration of the systems and then they were subjected to the continuous expansion in the z-direction with the rate 10^{-3} Å/ps. The x and y dimensions of the simulation box were coupled and controlled by the Nose-Hoover barostat so that the total pressure was constant during deformation of the simulation box. The resulting strain was computed as the relative expansion of the CNT length δl and the associated stress was computed as the zz components of the stress tensor summed over all atoms within the nanotube and divided by the nanotube volume. In that way the stress-strain curves were determined until the CNT fracture happened and the sudden drop in a given stress-strain plot occurred. The related strain and stress are counted as failure strain and ultimate stress, respectively. The Young modulus, according to Hooke's law, was determined as the slope of the stress-strain plot in an early stage of loading, i.e. up to 3%.

3. Results and discussion

3.1. Quantum chemical analysis of EB adsorption on the CNT surface

Experimental data concerning adsorption of the considered bisazo dyes on carbon nanotubes suggest that these molecules may alter the mechanical properties of the nanotubes leading to their shortening during sonication. Thus, it was necessary to carry out quantum chemical

calculations in order to check whether the adsorption has really a strongly chemical nature or it is rather a common physical process. Because the full CNT-dye-water system is not tractable using the quantum chemical methods we focused on a simplified but still representative model. Thus, we took the (17,0) carbon nanotube which diameter is very close to the nanotubes studied experimentally and a single EB molecule. In water solution EB exists in anionic form due to deprotonation of the sulfonate groups. However, in quantum chemical DFT calculations we had to use its neutral unprotonated form since we cannot account for the presence of explicit water.

Taking into account the azo-hydrazone tautomerism of organic azo dyes, as mentioned it already, we initially performed calculations for three possible tautomers of EB in the gas phase. Namely, azo/azo, azo/hydrazone and hydrazone/hydrazone forms. In addition, all these tautomers were incorporated to the mixed EB/CNT(17,0) system. Since the EB adsorption on the nanotube is driven by the $\pi - \pi$ stacking interactions combined with the formation of weak hydrogen bonds and according to the previous results [30] the maximal energetic effect is reached when the adsorbate interacts with the carbon nanotube by the largest possible contact area. Such a configuration was taken from a preliminary MD run.

In the DFT calculations all sulfonate groups in EB molecule were saturated by hydrogen and then the geometry optimization was carried out. The optimized structures of the azo/hydrazone and hydrazone/hydrazone tautomer on the nanotube are presented in Fig. 2A. Both in the gas and on the surface the azo/azo form was found as unfavorable and it easily transformed into the azo/hydrazone form. The latter is, in turn, less stable than the hydrazone/hydrazone one by 0.07 and 0.11 eV on CNT(17,0) and in the gas phase, respectively. The calculated E_{ads} are equal to −2.11 and −2.04 eV for the adsorption of the hydrazone/hydrazone and azo/hydrazone of EB on the CNT(17,0), respectively. Both values are, as seen, very similar and none of the forms seems to be a preferred one, especially at elevated temperatures and in aqueous solution.

The shortest distances between the carbon atoms from the aromatic rings of EB and CNT(17,0) are in the range 3.35–3.60 Å. Beside the $\pi - \pi$ stacking interactions, four hydrogen bonds of different strength between hydrogen from hydroxyl groups and carbon from the nanotube were created (2.19–3.91 Å). We utilized the charge density difference ($\Delta\rho(r)$), to indicate the nature of these bonds as shown in Fig. 2B, where the yellow (blue) color represents excess (deficient) regions of electron charge. The stronger intensity of the yellow and blue lobes (isovalue of $2 \cdot 10^{-4}$ e/Å^3) in the close vicinity of the sulfonyl hydroxide groups reveals the reorganization of electronic density due to the hydrogen bonds formation. However, these bonds do not exist in water solution due to deprotonation of sulfonyl groups. The hydrogen bond lengths (OH/NH donor and N/O acceptor) of the adsorbed hydrazone/hydrazone EB are equal to 1.610 and 1.991 Å, whereas in the case of an azo/hydrazone they are 1.62 and 1.86 Å. N-N bond lengths in the both adsorbed tautomers are in the range 1.28–1.31 Å, and these distances only marginally changed relative to those in the gas phase. To sum up, due to the low energy difference between both tautomers the intramolecular proton transfer can easily proceed. However, it cannot have any significant role in the adsorption behavior of EB molecule on the CNT surface at elevated temperature and in the presence of solvent. Therefore, the choice of a given tautomeric form of EB in construction of an empirical force field for molecular dynamics simulation is actually not important.

Finally, the influence of the adsorption of the EB (hydrazone/hydrazone) molecule on the electronic structure of the pristine CNT (17,0) is also presented. Fig. 3 shows the band structure and the total and projected DOS plot for the mixed system and the DOS plot for the pristine semiconducting nanotube as a reference. Although the GGA functionals underestimate the fundamental band gap, they are believed to correctly represent the character of the frontier orbitals and other low-laying states for different organic systems. [31] We found only a small shift in the Fermi level (the dash line in Fig. 3) by 0.12 eV after EB adsorption on CNT(17,0). The adsorbed molecule introduces a new state in the original gap of the pristine nanotube that corresponds to the LUMO level of the adsorbed molecule. The new bands are also located about 0.6 eV (the HOMO level of EB) below the Fermi level (−2.67 eV). When we compare the DOS plot close to the top of the valence band and to the bottom of the conduction band for the pristine and the molecule-adsorbed CNT(17,0), no difference is observed. Since the main interaction between the nanotube and the molecule is of electrostatic nature, only minor perturbation of the CNT(17,0) electronic structure appears.

The central conclusion drawn from quantum chemical DFT calculations is that the adsorption of EB has negligible influence on the chemical state of carbon nanotube. Therefore, the mechanical properties of the nanotubes are actually intact after adsorption of EB or perhaps also other bisazo dyes like Congo red, for instance.

Geometry optimization based on DFT calculations led to the structures shown in Fig. 2A. In Fig. 4, in turn, we compared the optimized structure from Fig. 2A (azo/hydrazone) and its analog obtained from classical molecular dynamics run using the AIREBO/gaff force field, as

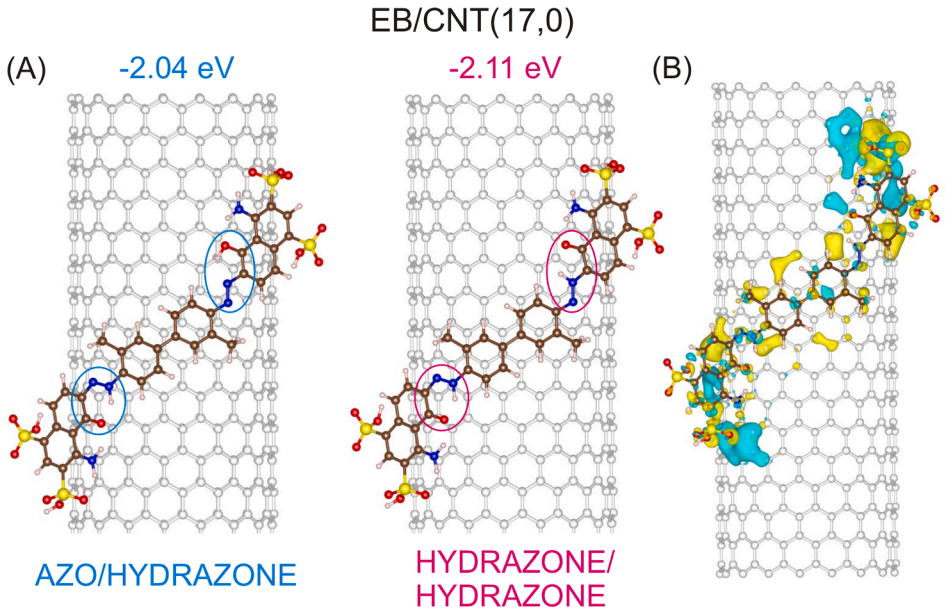

Fig. 2. (A) Optimized structures of the EB/CNT (17,0) system. Carbon atoms of the adsorbate are drawn in brown, nitrogen atoms in blue, oxygen atoms in red, sulfur atoms in yellow, and hydrogen atoms in pink. All carbon atoms from the nanotubes are in gray color for a better clarity of presentation. (B) Charge density difference ($\Delta\rho(r)$) after EB adsorption on CNT(17,0). The yellow (blue) lobe represents the electron excess (deficient) regions, i.e., the electron charge moved from the blue to the yellow regions. (For interpretation of the references to color in this figure legend, the reader is referred to the web version of this article.)

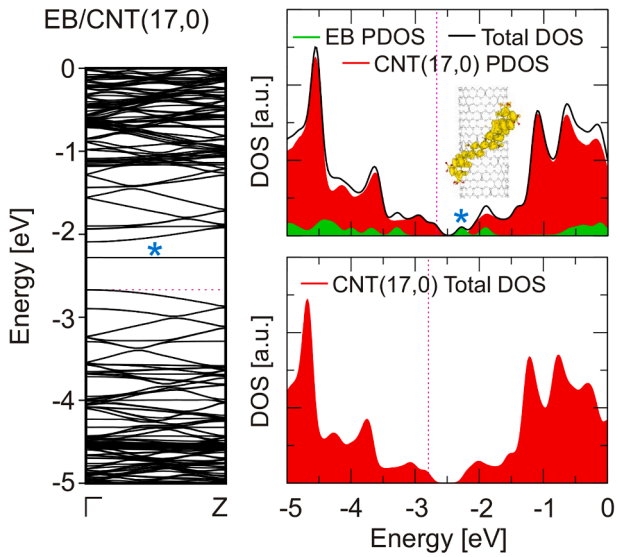

Fig. 3. Electronic band structure and total and projected density of states (DOS) obtained from the DFT(PBE) + D3(BJ) calculations for EB/CNT(17,0) and the pristine CNT(17,0). The Fermi level is marked by the dashed line. The corresponding electron density of the LUMO state of the adsorbed EB is also presented. The yellow surface represents an isovalue of 10^{-4} e/Å^3. (For interpretation of the references to color in this figure legend, the reader is referred to the web version of this article.)

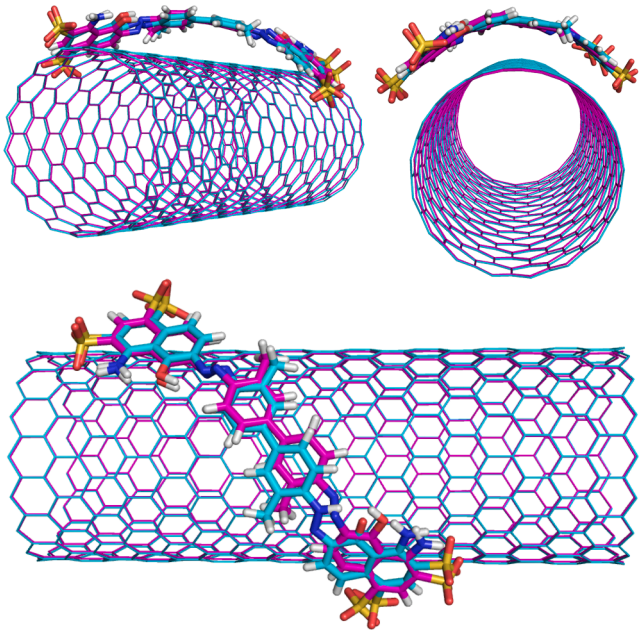

Fig. 4. Superimposition of the ab-initio optimized structure of EB/CNT(17,0) (dominating color cyan) and the structure obtained using classical molecular dynamics simulation with the AIREBO/gaff force field (dominating color magenta). The RMSD deviation (including hydrogen atoms) between them is only 0.335 Å. (For interpretation of the references to color in this figure legend, the reader is referred to the web version of this article.)

outlined in Section 2.2.4. Both structures were aligned to produce the best overlap and the RMSD between these two states was computed. The resulting RMSD value 0.335 Å means that the classical force field reproduces the ab-initio geometry very well and thus the classical force field will produce highly reliable results also in larger systems.

3.2. Fracture analysis of CNTs using molecular dynamics simulations

Classical molecular dynamics simulations with AIREBO/gaff force field were used for analysis of the mechanical properties of carbon nanotubes. Initial stages of simulations were devoted to generation of various types of nanotubes (bare, carboxyl functionalized and defective with two types of chirality) and equilibrations. Analysis of the structure of the adsorbed dyes, their energetics, ordering etc. were not performed because these kinds of problems have already been addressed, at least partially, in other publications [32,13,9]. Thus, further calculations were focused on the analysis of fracture phenomena and the associated parameters.

The fracture analyses were performed for all studied systems in order to check how the surface functionalization, temperature, presence of surface defects and particularly adsorption of CR and EB affects the Young modulus and other tensile parameters. The typical stress-strain curves for systems without the adsorbed CR/EB are shown in Fig. 5. For each system three independent simulations were carried out and the corresponding tensile parameters were averaged and collected in Table 2.

As expected and clearly seen in Fig. 5 the presence of surface defects strongly affect the tensile characteristics of the nanotubes. The hardiness of the CNTs is drastically reduced upon generation of surface defects. Additionally, it is clearly seen that CNT chirality has very important influence on the tensile strength and our results coincides well with the literature data [33,34,35]. The above conclusions are also supported by the failure strain and ultimate stress values determined from stress-strain plots and shown in Table 2.

Thus, the armchair nanotubes are more resistant to tensile failure than the zigzag ones and the presence of surface defects reduces their hardiness strongly. Also the Young modulus is reduced upon generation

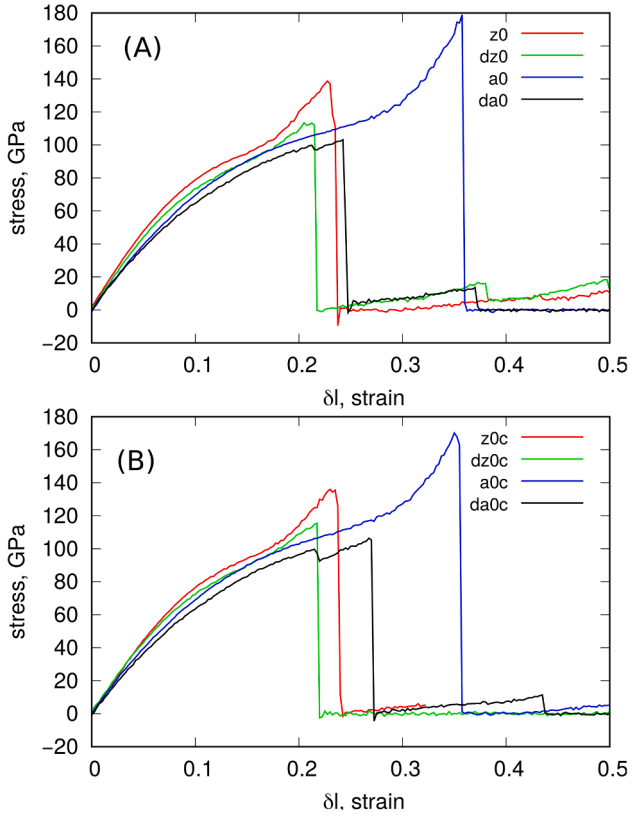

Fig. 5. Typical stress-strain curves for systems without the adsorbed CR/EB at temperature 298 K and without (A) or with (B) surface carboxyl functionalizations. The systems with the prefix 'd' have defective CNT as illustrated in Fig. 1C, D.

Table 2
Mean values of the tensile parameters determined for the studied systems at two temperatures.

System	Failure strain		Ultimate stress, GPa		Young modulus, GPa	
	298K	368K	298K	368K	298K	368K
z0	0.234 ± 0.002	0.232 ± 0.001	137 ± 2	136 ± 1	977 ± 9	965 ± 6
dz0	0.217 ± 0.004	0.208 ± 0.007	115 ± 2	111 ± 3	919 ± 14	908 ± 9
a0	0.357 ± 0.001	0.351 ± 0.004	178 ± 2	172 ± 6	849 ± 1	860 ± 5
da0	0.247 ± 0.012	0.254 ± 0.004	104 ± 5	105 ± 1	794 ± 7	793 ± 4
z0c	0.237 ± 0.002	0.233 ± 0.002	137 ± 1	134 ± 1	953 ± 1	951 ± 4
dz0c	0.218 ± 0.009	0.215 ± 0.003	113 ± 4	112 ± 2	879 ± 2	886 ± 4
a0c	0.348 ± 0.004	0.345 ± 0.003	166 ± 3	164 ± 3	843 ± 3	843 ± 15
da0c	0.259 ± 0.008	0.267 ± 0.028	109 ± 2	110 ± 5	774 ± 10	787 ± 10
z20	0.233 ± 0.002	0.231 ± 0.002	137 ± 1	135 ± 1	1043 ± 11	1020 ± 21
dz20	0.218 ± 0.002	0.209 ± 0.003	116 ± 2	110 ± 2	954 ± 46	934 ± 28
a20	0.347 ± 0.001	0.342 ± 0.001	168 ± 1	164 ± 1	900 ± 10	880 ± 15
da20	0.246 ± 0.036	0.243 ± 0.019	104 ± 7	104 ± 4	823 ± 20	838 ± 32
z20c	0.234 ± 0.001	0.232 ± 0.001	137 ± 1	134 ± 1	988 ± 16	986 ± 18
dz20c	0.223 ± 0.003	0.209 ± 0.008	113 ± 3	109 ± 4	945 ± 34	936 ± 21
a20c	0.345 ± 0.002	0.337 ± 0.003	163 ± 2	158 ± 3	900 ± 20	897 ± 6
da20c	0.247 ± 0.032	0.228 ± 0.023	107 ± 6	101 ± 6	799 ± 7	791 ± 21

of the surface defects and it is generally lower for armchair CNTs than for the zigzag ones. However, Young modulus in most cases seems to be slightly reduced after incorporation of the carboxyl groups onto the CNT surface. Another interesting observation is that the presence of surface covalent functionalization by carboxyl groups has little effect in modification of the failure strain and ultimate stress. But, there is an exception: these are the defective armchair nanotubes. It is seen in Table 2 that the failure strain reveals large fluctuations when compared to other cases. This means that fracture parameters in the case of the defective armchair nanotubes depend substantially on a local environment. Probably the state of water molecules or the adsorbed dyes invading the surface defect alter the overall mechanical properties of such types of nanotubes.

The systems 'da0′ and 'da0c' are visualized in Fig. 6. The other cases reveal similar fracture patterns. Thus, the fracture propagates around the surface defect in cases of defective nanotubes and the atoms forming the edge of the hole easily migrate and exchange the localization with other atoms. This is fully understandable since in the area close to the defect the nanotube is mechanically weakened. However, as seen in Fig. 5 or in Table 2 the presence of carboxyl groups (or just sp3 carbon atoms) in the vicinity of the defect slightly enhances the mechanical strength, as reflected by the larger values of the failure strain. Non-defected CNTs break in random places and the presence of carboxyl groups has actually minor effect in their tensile parameters values.

Fig. 7 shows the stress-strain curves for analogous systems but with the adsorbed CR/EB on the nanotubes surfaces. As found in the DFT studies adsorption of EB on the nanotube (17,0) has minimal effect in terms of the chemical properties of CNT. Therefore, the MD model based on classical AIREBO/gaff force fields is fully adequate in describing physical (or mechanical forces) effects related to adsorption of CR/EB on

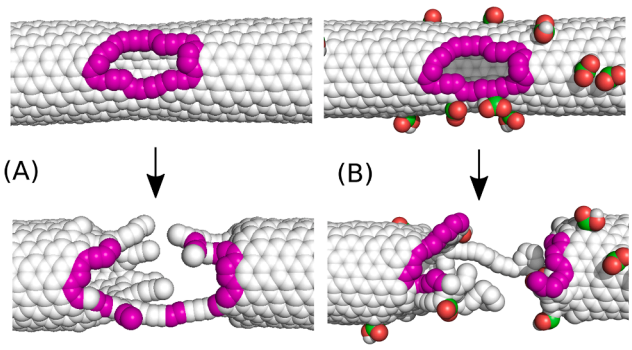

Fig. 6. Visualization of the CNT structures just before fracture at temperature 298 K (top panels) and just after fracture (bottom panels) for (A): 'da0′ system and (B) 'da0c' system. Carbon atoms forming the edge of the hole (defect) are in magenta color. (For interpretation of the references to color in this figure legend, the reader is referred to the web version of this article.)

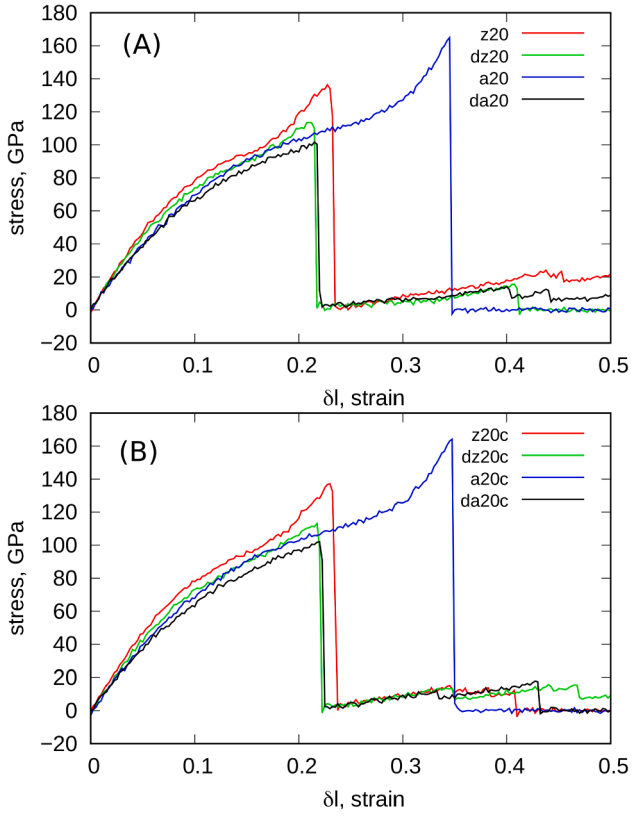

Fig. 7. Typical stress-strain curves for systems with the adsorbed CR/EB, determined at 298 K, and without (A) or with (B) surface carboxyl functionalizations. The systems with the prefix 'd' have defective CNT as illustrated in Fig. 1C, D.

the CNT surfaces.

By comparing Fig. 5 and Fig. 7 we can see that the adsorbed layer of CR/EB mixture on the CNT surface has rather small influence on the fracture parameters of carbon nanotube. Also the visualizations in Figs. 6 and 8 do not indicate visible differences between fracture patterns of nanotubes with and without dyes adsorbed. Of course, there is some mechanical force exerted on the carbon atoms as seen in more scattered stress-strain plots but the fracture parameters are not drastically changed. However, some changes appear and their discussion is more reliable when analyzing parameters values collected in Table 2 and Fig. 9, which directly shows how a given parameter has been changed

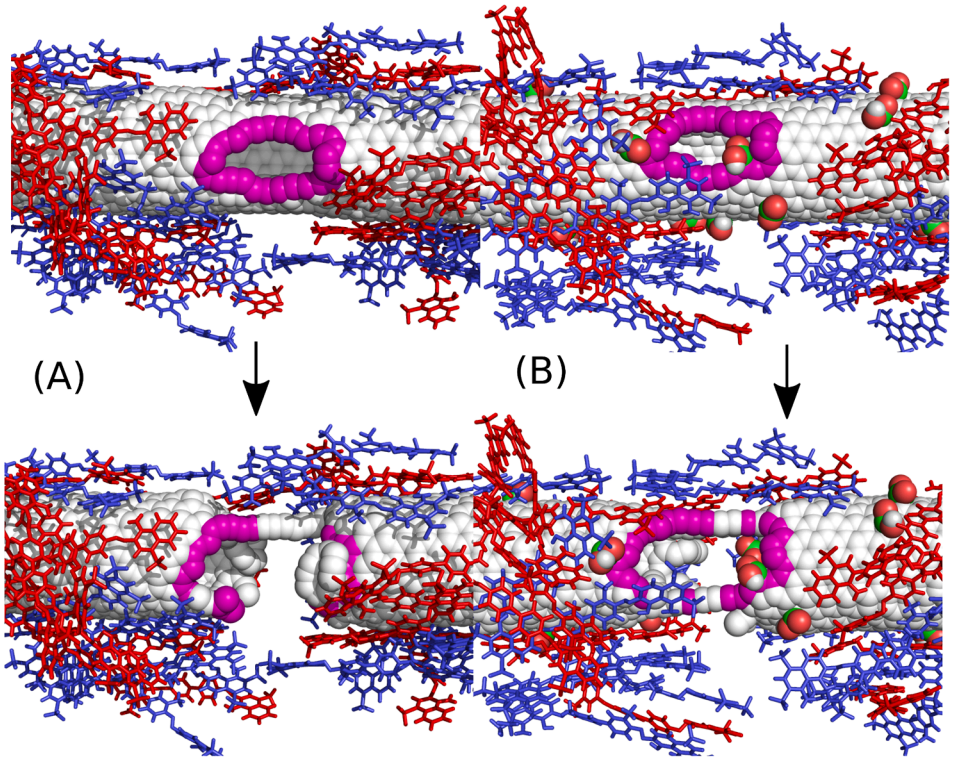

Fig. 8. Visualization of the CNT structures just before fracture at temperature 298 K (top panels) and just after fracture (bottom panels) for (A): 'da20' system and (B) 'da20c' system. Carbon atoms forming the edge of the hole (defect) are in magenta color while red and blue sticks correspond to CR and EB molecules, respectively. (For interpretation of the references to color in this figure legend, the reader is referred to the web version of this article.)

after adsorption of CR/EB.

The failure strain is actually unchanged in the case of zigzag nanotubes since the variations of that value are well below 5%. Armchair nanotubes do not reveal significant changes of the failure strain as well. But in some cases there are quite pronounced changes of the failure strain after adsorption of CR/EB. The changes are quite large in the case of defective armchair nanotubes (especially at elevated temperature 368 K). Additionally this type of the nanotubes reveal strong fluctuations of the failure strain values as shown in Table 2. This means that armchair nanotubes can undergo cleavage easier when the CR/EB are adsorbed on their surfaces but the necessary condition is the simultaneous presence of surface defects. The shortening of zigzag nanotubes is not facilitated by the adsorption of dyes no matter whether the nanotube is defective or not. Very similar conclusions can be drawn for the changes of the ultimate stress; the armchair nanotubes reveal the strongest reduction of that value due to adsorption of dyes though the changes are still rather small. The reduction of the tensile strength after adsorption of the dyes, observed mainly in defective armchair nanotubes, is probably due to partial intrusion of the dyes molecules in the surface defects/holes. However, this mechanism is not operative in the case of zigzag nanotubes perhaps due to their higher stiffness. Finally, the slightly reduced failure strain observed in the case of the armchair nanotube (a) without surface modification is quite difficult to explain. Probably the forces coming from the adsorbed dyes and exerted on the carbon atoms in the nanotube facilitate a faster failure of those nanotubes.

Changes of the Young modulus after adsorption of dyes is generally significant (sometimes more than 5%) in all of the cases. The observed increase of the Young modulus is probably related to somewhat reduced flexibility of the nanotubes in the directions perpendicular to the CNT axis. That reduction is caused by the surrounding layer of dyes molecules.

The effect of carboxyl groups in the fracture parameters was already mentioned but Fig. 10 represents those data in a more illustrative way. So, we can see that carboxyl groups affect the failure strain only minimally and the changes actually fit within the estimation error. However, we can note that the highest changes are observed in the case of defective armchair nanotubes. But their effect is different depending on the presence of the adsorbed CR/EB. Without the dyes the carboxyl groups enhance the nanotube strength but in the case of the dyes adsorbed on the CNT surface the carboxyl groups reduce (368 K) or do not affect (298 K) the strength. Thus, the shortening of defective armchair nanotubes is probably facilitated by the adsorption of dyes. As already mentioned the ultimate stress reveals similar changes like the failure strain and generally the armchair nanotubes are most sensitive to the presence of such factors like carboxyl functionalization or adsorption of dyes. Young modulus is generally reduced when the carboxyl groups are present on the nanotube surfaces. However, these changes are small and fit within the estimation error.

The effect of temperature on the values of tensile parameters can be easily deduced from the data in Table 2. Thus, we can see that failure strain and other parameters are almost unaffected by the increase of temperature from 298 K to 368 K. More detailed analysis can lead to the conclusion that there is small decrease of the values of the failure strain in cases where the standard deviation is small. Thus, the temperature increase slightly facilitates the fracture of the nanotubes. In the case of defective armchair nanotubes the situation is not so clear since the mean values of the failure strain are accompanied by high estimation errors.

The behavior of armchair nanotubes under the tensile load is however intriguing and deserves further more detailed studies. Particularly the effects produced by the surface defect are interesting and it would be valuable to carry out a dedicated DFT studies focused on the nature of the interaction of EB with defective nanotubes. Perhaps the dangling bonds, though formally inactive in classical MD, may reveal an enhanced reactivity in contact with EB and the cleavage of CNTs can be still facilitated (or even generated in the case of zigzag nanotubes). However, the defect structure (size, shape) can have important implications in the course of DFT computations. This, in turn, requires a

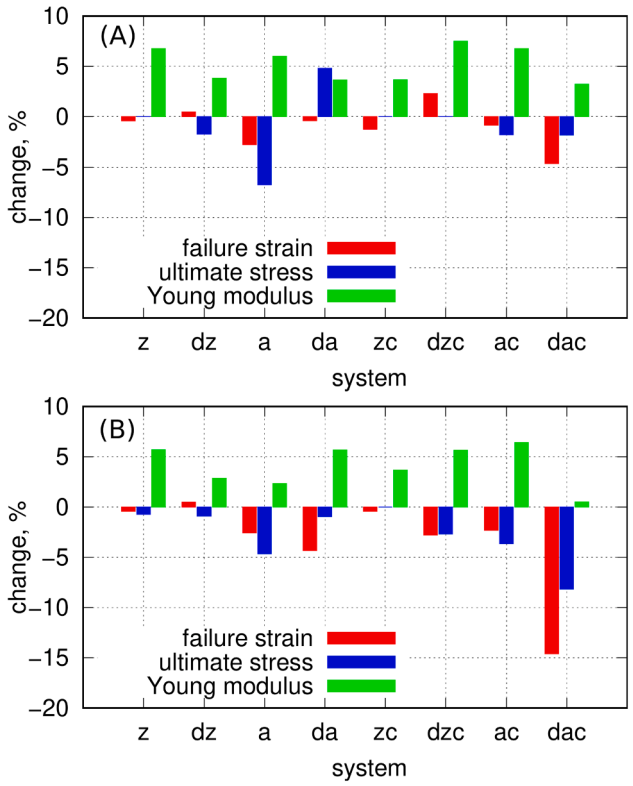

Fig. 9. Changes of the failure strain, ultimate stress and Young modulus after adsorption of the CR/EB mixture. The percentage change is calculated in reference to a given system without the CR/EB adsorbed. The systems names are following: z - zigzag nanotube, a - armchair nanotube, d - defected and c - carboxyl functionalized nanotube. Part (A) corresponds to temperature 298 K while part (B) is for temperature 368 K.

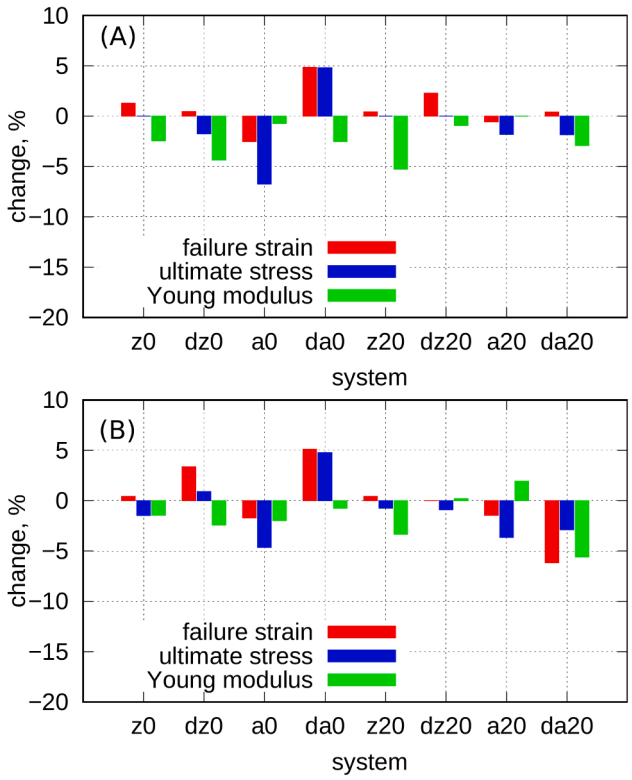

Fig. 10. Changes of the failure strain, ultimate stress and Young modulus due to incorporation of carboxyl groups to the CNT surface. The percentage change is calculated in reference to a given system without the carboxyl groups. The systems names are following: z - zigzag nanotube, a - armchair nanotube, d - defected and 0 - without dyes adsorbed, 20 - with dyes adsorbed. Part (A) concerns the temperature 298 K while part (B) is for temperature 368 K.

number of various cases/systems processed by the DFT method and, due to high computational costs of such type of calculations, this will be a matter of dedicated studies.

Nevertheless the results discussed above partially explain the experimental observations concerning the shortening of the nanotubes due to adsorption of CR/EB mixture [8]. It was experimentally found that addition of CNT suspension to CR/EB mixture and sonication led to straightening and shortening of the nanotubes from 1–2 mm to 300–400 nm in length. A control sample, with sodium cholate as dispersion agent, did not show such an effect. Moreover, the adsorbed CR/EB clusters were identified at the ends of the shortened nanotubes which suggests that the fracture occurred at places where the dyes were attached. We have already found in molecular dynamics simulations that CR (or CR/doxorubicin mixture) attach to the CNT surface in a form of big supramolecular clusters [32,36] thus it is likely that those clusters move on the CNT surface and sometimes meet defective areas. Taking into account that sonication deliver huge mechanical energy to the system we could assume that fracture of the nanotubes occurs at those defective sites since the failure strain is then significantly (by ca. 15% at 368 K) reduced, as shown in Fig. 9. But the above mechanism should be operative for armchair nanotubes only. On the other hand the experimental results do not distinguish the CNT chirality but definitely they are not pure armchair ones. Therefore, we suppose that all nanotubes types can be broken by the mechanical energy coming from sonication and the presence of big CR/EB clusters, probably attached to the CNT close to surface defects, mechanically facilitate the fracture of the nanotubes. Our quantum chemical studies do not imply any specific chemical deterioration of the nanotube structure due to adsorption of EB on a perfect CNT. Thus, molecular dynamics simulations suggest that the only effect, if any, may be due to mechanical forces coming from the adsorbed heavy clusters of CR/EB and having measurable effect only in defective nanotubes.

4. Summary and conclusions

This study focused on the two aspects of the interaction of bisazo dyes, particularly CR and EB, with carbon nanotubes. The first aspect was the nature of the interaction of the dyes molecules with the CNT that is whether the interaction is of chemical type leading to substantial modification of the electronic structure of nanotubes or it is just a common physical adsorption. The ab-initio DFT calculations results led to the conclusion that adsorption of EB molecule on the (17,0) carbon nanotube does not lead to substantial changes of the density of states and the position of the Fermi level. Two tautomeric forms of EB were detected but the difference in internal or adsorption energy between them was small. Another important conclusion coming from quantum chemical studies was the observation that the optimized structure of EB on the (17,0) is almost identical like the structure obtained from classical molecular dynamics simulations with the AIREBO/gaff force field.

The second aspect of the study was the analysis of carbon nanotubes fracture phenomena. The aim of that study was the understanding the role of various factors in modification of the mechanical parameters of the nanotubes. The AIREBO/gaff force field was used in molecular dynamic simulations of the tensile load of carbon nanotubes with the adsorbed CR/EB in aqueous solution. Two types of chiralities were studied (17,0) and (10,10) and the nanotubes were also additionally functionalized by carboxyl groups. We also studied the role of surface defects in modification of the mechanical properties of carbon nanotubes.

Analysis of fracture parameters values under the tensile load led to

following conclusions: zigzag nanotubes are not sensitive to covalent functionalization by carboxyl groups or adsorption of CR/EB on their surfaces. Only the Young modulus was slightly affected by those factors. However, the presence of surface defects strongly reduces either the failure strain or the ultimate stress. On the contrary, the armchair nanotube reveal some changes of the failure strain or other tensile parameters after incorporation of carboxyl groups or even being the effect of CR/EB adsorption. However, these changes appear for defective armchair nanotubes; the non-defective ones either do not reveal substantial alteration of the fracture parameters or the changes are only very modest.

The obtained results generally do not support the hypothesis that adsorption of bisazo dyes on the CNT surfaces leads to their shortening due to strong chemical modification of their properties. Such a conclusion could be drawn for defective armchair nanotubes but again the reduction of the failure strain due to adsorption of CR/EB has rather physical than a chemical background. The experimentally observed shortening of the CNT during sonication with the adsorbed CR/EB mixture (or CR/doxorubicin) should also be classified as a physical effect. We suppose that tendency to formation of isolated big supramolecular clusters on the nanotube surfaces by bisazo dyes leads to huge mechanical strain during sonication and that strain is enough for fracture of all nanotubes types. The key factor is the presence of large heavy clusters of dyes sitting on the nanotube in a long axial separation, perhaps located in defective areas of the nanotube.

CRediT authorship contribution statement

Anna Jagusiak: Conceptualization, Methodology, Investigation, Visualization, Funding acquisition, Writing - review & editing. **Jakub Goclon:** Conceptualization, Methodology, Software, Formal analysis, Writing - review & editing, Visualization. **Tomasz Panczyk:** Conceptualization, Methodology, Investigation, Visualization, Software, Writing - original draft, Visualization, Supervision.

Declaration of Competing Interest

The authors declare that they have no known competing financial interests or personal relationships that could have appeared to influence the work reported in this paper.

Acknowledgments

The periodic DFT calculations were carried out using the PLGrid Infrastructure. The computations were performed on Prometheus supercomputer at ACC Cyfronet AGH-UST.

A. J. thanks National Science Centre Poland (NCN) for financial support (grant no. 2016/21/D/NZ1/02763).

Appendix A. Supplementary data

Supplementary data to this article can be found online at https://doi.org/10.1016/j.apsusc.2020.148236.

References

[1] M.R. Mananghaya, G.N. Santos, D. Yu, Solubility of aminotriethylene glycol functionalized single wall carbon nanotubes: A density functional based tight binding molecular dynamics study: Solubility of Aminotriethylene Glycol Functionalized Single Wall Carbon Nanotubes: A Density Functional Based Tight Binding Molecular Dynamics Study, J. Comput. Chem. 40 (2019) 952–958, https://doi.org/10.1002/jcc.25776.

[2] M.R. Mananghaya, G.N. Santos, D.N. Yu, Solubility of amide functionalized single wall carbon nanotubes: a quantum mechanical study, J. Mol. Liq. 242 (2017) 1208–1214, https://doi.org/10.1016/j.molliq.2017.07.107.

[3] S. Morales-Torres, T.L.S. Silva, L.M. Pastrana-Martínez, A.T.S.C. Brandão, J. L. Figueiredo, A.M.T. Silva, Modification of the surface chemistry of single- and multi-walled carbon nanotubes by HNO_3 and H_2SO_4 hydrothermal oxidation for application in direct contact membrane distillation, Phys. Chem. Chem. Phys. 16 (2014) 12237–12250, https://doi.org/10.1039/C4CP00615A.

[4] S.C. Tsang, P.J.F. Harris, M.L.H. Green, Thinning and opening of carbon nanotubes by oxidation using carbon dioxide, Nature 362 (1993) 520–522, https://doi.org/10.1038/362520a0.

[5] D.B. Mawhinney, V. Naumenko, A. Kuznetsova, J.T. Yates, J. Liu, R.E. Smalley, Infrared spectral evidence for the etching of carbon nanotubes: ozone oxidation at 298 K, J. Am. Chem. Soc. 122 (2000) 2383–2384, https://doi.org/10.1021/ja994094s.

[6] K. Kan, T. Xia, L. Li, H. Bi, H. Fu, K. Shi, Amidation of single-walled carbon nanotubes by a hydrothermal process for the electrooxidation of nitric oxide, Nanotechnology. 20 (2009) 185502, https://doi.org/10.1088/0957-4484/20/18/185502.

[7] M. Kierkowicz, E. Pach, A. Santidrián, S. Sandoval, G. Gonçalves, E. Tobías-Rossell, M. Kalbáč, B. Ballesteros, G. Tobias, Comparative study of shortening and cutting strategies of single-walled and multi-walled carbon nanotubes assessed by scanning electron microscopy, Carbon 139 (2018) 922–932, https://doi.org/10.1016/j.carbon.2018.06.021.

[8] A. Jagusiak, B. Piekarska, K. Chłopaś, E. Bielańska, T. Pańczyk, Shortening and dispersion of single-walled carbon nanotubes upon interaction with mixed supramolecular compounds, Bio-Algorithms and Med-Systems 12 (2016), https://doi.org/10.1515/bams-2016-0015.

[9] A. Jagusiak, B. Piekarska, T. Pańczyk, M. Jemioła-Rzemińska, E. Bielańska, B. Stopa, G. Zemanek, J. Rybarska, I. Roterman, L. Konieczny, Dispersion of single-wall carbon nanotubes with supramolecular Congo red – properties of the complexes and mechanism of the interaction, Beilstein J. Nanotechnol. 8 (2017) 636–648, https://doi.org/10.3762/bjnano.8.68.

[10] E.I. Yakupova, L.G. Bobyleva, I.M. Vikhlyantsev, A.G. Bobylev, Congo Red and amyloids: history and relationship, Bioscience Reports. 39 (2019) BSR20181415. https://doi.org/10.1042/BSR20181415.

[11] C.J.O.R. Morris, The determination of plasma volume by the Evans blue method: the analysis of haemolysed plasma, J. Physiol. 102 (1944) 441–445, https://doi.org/10.1113/jphysiol.1944.sp004049.

[12] B.S. Wong, S.L. Yoong, A. Jagusiak, T. Panczyk, H.K. Ho, W.H. Ang, G. Pastorin, Carbon nanotubes for delivery of small molecule drugs, Adv. Drug Deliv. Rev. 65 (2013) 1964–2015, https://doi.org/10.1016/j.addr.2013.08.005.

[13] A. Jagusiak, T. Pańczyk, Interaction of Congo Red, Evans Blue and Titan Yellow with doxorubicin in aqueous solutions. A molecular dynamics study, J. Mol. Liquids 279 (2019) 640–648, https://doi.org/10.1016/j.molliq.2019.02.012.

[14] S.J. Stuart, A.B. Tutein, J.A. Harrison, A reactive potential for hydrocarbons with intermolecular interactions, J. Chem. Phys. 112 (2000) 6472, https://doi.org/10.1063/1.481208.

[15] J. Wang, W. Wang, P.A. Kollman, D.A. Case, Automatic atom type and bond type perception in molecular mechanical calculations, J. Mol. Graph. Model. 25 (2006) 247–260, https://doi.org/10.1016/j.jmgm.2005.12.005.

[16] https://www.quantum-espresso.org/, (n.d.).

[17] D. Vanderbilt, Soft self-consistent pseudopotentials in a generalized eigenvalue formalism, Phys. Rev. B. 41 (1990) 7892–7895, https://doi.org/10.1103/PhysRevB.41.7892.

[18] J.P. Perdew, K. Burke, M. Ernzerhof, Generalized gradient approximation made simple, Phys. Rev. Lett. 77 (1996) 3865–3868, https://doi.org/10.1103/PhysRevLett.77.3865.

[19] S. Grimme, S. Ehrlich, L. Goerigk, Effect of the damping function in dispersion corrected density functional theory, J. Comput. Chem. 32 (2011) 1456–1465, https://doi.org/10.1002/jcc.21759.

[20] R. Fletcher, Practical methods of optimization, second ed., reprinted in paperback, June 2008, Wiley, Chichester, 2008.

[21] H.J. Monkhorst, J.D. Pack, Special points for Brillouin-zone integrations, Phys. Rev. B 13 (1976) 5188–5192, https://doi.org/10.1103/PhysRevB.13.5188.

[22] P. Ball, C.H. Nicholls, Azo-hydrazone tautomerism of hydroxyazo compounds—a review, Dyes Pigm. 3 (1982) 5–26, https://doi.org/10.1016/0143-7208(82)80010-7.

[23] K. Momma, F. Izumi, *VESTA 3* for three-dimensional visualization of crystal, volumetric and morphology data, J. Appl. Crystallogr. 44 (2011) 1272–1276, https://doi.org/10.1107/S0021889811038970.

[24] A. Kokalj, Computer graphics and graphical user interfaces as tools in simulations of matter at the atomic scale, Computational Mater. Sci. 28 (2003) 155–168, https://doi.org/10.1016/S0927-0256(03)00104-6.

[25] A.W. Sousa da Silva, W.F. Vranken, ACPYPE - AnteChamber PYthon Parser interfacE, BMC Res. Notes 5 (2012) 367, https://doi.org/10.1186/1756-0500-5-367.

[26] https://ambermd.org/AmberTools.php, AmberTools, (n.d.). https://ambermd.org/AmberTools.php (accessed June 17, 2020).

[27] H.J.C. Berendsen, D. van der Spoel, R. van Drunen, GROMACS: A message-passing parallel molecular dynamics implementation, Comput. Phys. Commun. 91 (1995) 43–56, https://doi.org/10.1016/0010-4655(95)00042-E.

[28] D.W. Brenner, O.A. Shenderova, J.A. Harrison, S.J. Stuart, B. Ni, S.B. Sinnott, A second-generation reactive empirical bond order (REBO) potential energy expression for hydrocarbons, J. Phys.: Condens. Matter 14 (2002) 783–802, https://doi.org/10.1088/0953-8984/14/4/312.

[29] S. Plimpton, Fast parallel algorithms for short-range molecular dynamics, J. Comput. Phys. 117 (1995) 1–19, https://doi.org/10.1006/jcph.1995.1039.

[30] J. Goclon, M. Kozlowska, P. Rodziewicz, Noncovalent functionalization of single-walled carbon nanotubes by aromatic diisocyanate molecules: a computational study, Chem. Phys. Lett. 598 (2014) 10–16, https://doi.org/10.1016/j.cplett.2014.02.042.

[31] T.P. Kaloni, G. Schreckenbach, M.S. Freund, Band gap modulation in polythiophene and polypyrrole-based systems, Sci. Rep. 6 (2016) 36554, https://doi.org/10.1038/srep36554.
[32] T. Panczyk, P. Wolski, A. Jagusiak, M. Drach, Molecular dynamics study of Congo red interaction with carbon nanotubes, RSC Adv. 4 (2014) 47304–47312, https://doi.org/10.1039/C4RA06806H.
[33] L.G. Zhou, S.Q. Shi, Molecular dynamic simulations on tensile mechanical properties of single-walled carbon nanotubes with and without hydrogen storage, Comput. Mater. Sci. 23 (2002) 166–174, https://doi.org/10.1016/S0927-0256(01)00233-6.
[34] K. Mylvaganam, L.C. Zhang, Important issues in a molecular dynamics simulation for characterising the mechanical properties of carbon nanotubes, Carbon 42 (2004) 2025–2032, https://doi.org/10.1016/j.carbon.2004.04.004.
[35] S. Ajori, S.H. Boroushak, R. Ansari, Fracture analysis and tensile properties of perfect and defective carbon nanotubes functionalized with carbene using molecular dynamics simulations, J. Braz. Soc. Mech. Sci. Eng. 42 (2020) 450, https://doi.org/10.1007/s40430-020-02530-z.
[36] A. Jagusiak, K. Chlopas, G. Zemanek, P. Wolski, T. Panczyk, Controlled release of doxorubicin from the drug delivery formulation composed of single-walled carbon nanotubes and Congo red: a molecular dynamics study and dynamic light scattering analysis, Pharmaceutics 12 (2020) 622, https://doi.org/10.3390/pharmaceutics12070622.